



HAL
open science

From zero to infinity: Minimum to maximum diversity of the planet by spatio-parametric Rao's quadratic entropy

Duccio Rocchini, Matteo Marcantonio, Daniele da Re, Giovanni Bacaro, Enrico Feoli, Giles Foody, Reinhard Furrer, Ryan Harrigan, David Kleijn, Martina Iannacito, et al.

► To cite this version:

Duccio Rocchini, Matteo Marcantonio, Daniele da Re, Giovanni Bacaro, Enrico Feoli, et al.. From zero to infinity: Minimum to maximum diversity of the planet by spatio-parametric Rao's quadratic entropy. *Global Ecology and Biogeography*, 2021, 30 (5), pp.1153-1162. 10.1111/geb.13270 . hal-03363010

HAL Id: hal-03363010

<https://hal.science/hal-03363010>

Submitted on 3 Nov 2021

HAL is a multi-disciplinary open access archive for the deposit and dissemination of scientific research documents, whether they are published or not. The documents may come from teaching and research institutions in France or abroad, or from public or private research centers.

L'archive ouverte pluridisciplinaire **HAL**, est destinée au dépôt et à la diffusion de documents scientifiques de niveau recherche, publiés ou non, émanant des établissements d'enseignement et de recherche français ou étrangers, des laboratoires publics ou privés.

From zero to infinity: Minimum to maximum diversity of the planet by spatio-parametric Rao's quadratic entropy

Duccio Rocchini^{1,2}, Matteo Marcantonio³, Daniele Da Re⁴, Giovanni Bacaro⁵, Enrico Feoli⁵, Giles M. Foody⁶, Reinhard Furrer⁷, Ryan J. Harrigan⁸, David Kleijn⁹, Martina Iannacito¹⁰, Jonathan Lenoir¹¹, Meixi Lin¹², Marco Malavasi², Elisa Marchetto¹, Rachel S. Meyer¹², Vítězslav Moudry², Fabian D. Schneider¹³, Petra Šímová², Andrew H. Thornhill^{14,15}, Elisa Thouverai¹, Saverio Vicario¹⁶, Robert K. Wayne¹², Carlo Ricotta¹⁷

¹BIOME Lab, Department of Biological, Geological and Environmental Sciences, Alma Mater Studiorum University of Bologna, Bologna, Italy

²Department of Spatial Sciences, Faculty of Environmental Sciences, Czech University of Life Sciences Prague, Praha - Suchbátka, Czech Republic

³Department of Pathology, Microbiology, and Immunology, School of Veterinary Medicine, University of California, Davis, California, USA

⁴Georges Lemaître Center for Earth and Climate Research, Earth and Life Institute, UCLouvain, Louvain-la-Neuve, Belgium

⁵Department of Life Sciences, University of Trieste, Trieste, Italy

⁶School of Geography, University of Nottingham, Nottingham, UK

⁷Department of Mathematics and Department of Computational Science, University of Zurich, Zurich, Switzerland

⁸Center for Tropical Research Institute of the Environment and Sustainability, University of California-Los Angeles, Los Angeles, California, USA

⁹Plant Ecology and Nature Conservation Group, Wageningen University, Wageningen, The Netherlands

¹⁰Inria Bordeaux - Sud-Ouest, Talence, France

¹¹UR "Ecologie et Dynamique des Systèmes Anthropisés" (EDYSAN, UMR 7058 CNRS-UPJV), Université de Picardie Jules Verne, Amiens, France

¹²Department of Ecology and Evolutionary Biology, University of California-Los Angeles, Los Angeles, California, USA

¹³Jet Propulsion Laboratory, California Institute of Technology, Pasadena, California, USA

¹⁴Environment Institute, The University of Adelaide, Adelaide, South Australia, Australia

¹⁵Department for Environment and Water, State Herbarium of South Australia, Botanic Gardens and State Herbarium, Adelaide, South Australia, Australia

¹⁶Institute of Atmospheric Pollution Research–Italian National Research Council C/O
Department of Physics, University of Bari, Italy

¹⁷Department of Environmental Biology, University of Rome “La Sapienza”, Rome, Italy

1
2
3
4
5
6
7
8
9
10 1 From zero to infinity: minimum to maximum diversity
11
12
13
14 2 of the planet by spatio-parametric Rao's quadratic
15
16
17
18 3 entropy
19
20
21
22
23 4
24
25
26 5 November 8, 2020
27
28
29
30
31 6

32
33
34
35
36
37
38
39
40
41
42
43
44
45
46
47
48
49
50
51
52
53
54
55
56
57
58
59
60

7
8
9
10
11
12
13
14
15
16
17
18
19

Abstract

Aim: The majority of work done to gather information on Earth diversity has been carried out by in-situ data, with known issues related to epistemology (e.g., species determination and taxonomy), spatial uncertainty, logistics (time and costs), among others. An alternative way to gather information about spatial ecosystem variability is the use of satellite remote sensing. It works as a powerful tool for attaining rapid and standardized information. Several metrics used to calculate remotely sensed diversity of ecosystems are based on Shannon's Information Theory, namely on the differences in relative abundance of pixel reflectances in a certain area. Additional metrics like the Rao's quadratic entropy allow the use of spectral distance beside abundance, but they are point descriptors of diversity, namely they can account only for a part of the whole diversity continuum. The aim of this paper is thus to generalize the Rao's quadratic entropy by proposing its parameterization for the first time.

1
2
3
4 20 **Innovation:** The parametric Rao's quadratic entropy, coded in R, i) allows to
5
6 21 represent the whole continuum of potential diversity indices in one formula, and ii)
7
8 22 starting from the Rao's quadratic entropy, allows to explicitly make use of distances
9
10 23 among pixel reflectance values, together with relative abundances.

11
12 24 **Main conclusions:** The proposed unifying measure is an integration between
13
14 25 abundance- and distance-based algorithms to map the continuum of diversity given
15
16
17 26 a satellite image at any spatial scale.

18
19
20 27 *Keywords:* biodiversity; ecological informatics; modelling; remote sensing; satellite
21
22
23 28 imagery.

24
25 29
26
27
28
29
30
31
32
33
34
35
36
37
38
39
40
41
42
43
44
45
46
47
48
49
50
51
52
53
54
55
56
57
58
59
60

1 Introduction

Since Alexander von Humboldt (1769-1859), the spatial component of nature has played a relevant role in natural science. In the development of theoretical and empirical models in ecology, spatial structure represents a key concept to allow scientists to link ecological patterns to the generating processes and to the functional networking among organisms (Borcard and Legendre, 2002).

The majority of the work done to gather information about Earth diversity has been carried out by in-situ data, with known issues related to epistemology (e.g., species determination and taxonomy), spatial uncertainty, logistics (time and costs), among others (Rocchini et al., 2011).

Using satellite remote sensing can at least help attaining rapid and standardized information about Earth diversity (Gillespie, 2005; Rocchini et al., 2005). Furthermore, remote sensing can also be used to monitor some ecosystem functions and parameters such as temperatures, photosynthesis, vegetation biomass production and precipitation (Schimel et al., 2019; Zellweger et al., 2019) that can be useful to define the different niches of in-situ species, following first Goodall (1970) ideas, who envisaged future diversity measures as those based on niche theory (Hutchinson, 1959). The free access to remote sensing data (see Zellweger et al., 2019) has opened new ways to study ecosystem diversity and biodiversity issues (Rocchini et al., 2013). The spectral data related to pixels, as operational geographical units, are descriptions of pieces of land that allow us to define a new kind of Earth “diversity”, which may complement in-situ biodiversity measurement.

Diversity varies with area, thus investigating multiple spatial grains, until wide extents, is important to effectively monitor spatial diversity change in space and time (MacArthur et al., 1966). This is especially true in macroecology, where the primary aim

1
2
3
4 54 is to model large-scale spatial patterns to infer the ecological processes which generated
5
6 55 them, particularly considering the recent effect of global changes worldwide (Hobohm et
7
8 56 al., 2019). In order to determine the horizontal distribution of diversity within a satellite
9
10 57 image (i.e. which areas within the image are more diverse than others), diversity indices
11
12 58 are usually spatially referenced by calculating the index within a moving window.

13
14
15 59 Several metrics that measure diversity from satellites rely on the Shannon's theory of
16
17 60 entropy (Shannon, 1948), with diversity being measured as $H = -\sum_{i=1}^N p_i \log p_i$, where
18
19 61 p_i is the proportion of the i -th pixel value (e.g., digital number, DN) found within a
20
21 62 moving window containing N pixels. Shannon's H basically summarizes the partition of
22
23 63 abundances (*sensu* Whittaker, 1965) by taking into account both relative abundance and
24
25 64 richness of DNs (Figure 1).

26
27
28
29
30 65 However, Shannon's entropy is a point descriptor of (remotely sensed) diversity. As
31
32 66 such, it shows only one part of the whole potential diversity spectrum at a glance. The
33
34 67 use of generalized entropies has been advocated to face such problem. In this case, one
35
36 68 single formula represents a parameterized version of a diversity index, thus providing a
37
38 69 continuum of potential diversity indices. In the context of the measurement of diversity,
39
40 70 the Rényi (1970) parametric entropy

$$H_\alpha = \frac{1}{1-\alpha} \log \sum_{i=1}^N p_i^\alpha \quad (1)$$

41
42
43
44
45
46
47
48
49
50 71
51
52
53 72 with $0 \leq \alpha \leq \infty$ represents a powerful tool to account for the continuum of diversity
54
55 73 (Figure 1).

56
57
58 74 One particularly convenient property of H_α is that by varying the parameter α there
59
60 75 is a continuum of possible diversity measures, which differ in their sensitivity to rare and

1
2
3 abundant DNs, becoming increasingly dominated by the most common DNs for increasing
4
5 values of α . Note that for $\alpha \rightarrow 1$, H_1 equals the Shannon's entropy. A similar formulation
6
7 was then proposed by Hill (1973) who expressed parametric diversity as the "numbers
8
9 equivalent" of Rényi generalized entropy. Appendix S1 provides the original formulation.
10
11

12 Rényi (and Hill) parametric functions summarize diversity by taking into account the
13
14 pixel values of a satellite image and their relative abundances. However, they do not allow
15
16 to explicitly consider the differences among these values. As an example, two arrays of
17
18 9 pixels with maximum richness and evenness (i.e. both containing 9 different DNs with
19
20 relative abundances $p_i = \frac{1}{9}$) but differing in their values will attain the same Shannon
21
22 diversity irrespective of the values of the DNs in both arrays.
23
24
25

26 By introducing a distance parameter d_{ij} among each pair of values i and j , Rao's
27
28 quadratic entropy (Rao , 1982)
29
30
31

$$Q = \sum_{i,j=1}^N p_i p_j d_{ij} \quad (2)$$

32
33
34
35
36
37
38
39
40 explicitly considers the differences among the pixel values in the calculation of diversity
41
42 (Figure 1). Hence, two different pixels with values [2,3] will attain a lower diversity with
43
44 respect to two pixels with values [0,100]. For instance, to make an ecological parallel, this
45
46 is somewhat similar to the phylogenetic distance between two species: the values [2,3]
47
48 would be equivalent to two sister species closely related on the tree of life while [1,100]
49
50 would be equivalent to two very distant species on the tree of life.
51
52
53

54 The aim of this paper is thus to propose, for the first time, a parameterization of
55
56 Rao's quadratic entropy in order to provide a generalized entropy which accounts for
57
58 both relative abundances and distances among pixel values. The proposed approach is
59
60

1
2
3
4 98 now part of the rasterdiv R package, a package dedicated to diversity measures of
5
6 99 spatial matrices, increasing its capability to discern among different diversity measures
7
8 100 by a single formula.
9

101 2 Spatio-parametric Rao's quadratic entropy

102 Inter-pixel spectral distances are directly related to landscape heterogeneity and they
103 are capable of describing species habitats, starting with a satellite image (Rocchini et al.,
104 2005). A satellite image can be viewed as a matrix of numbers describing Earth reflectance
105 in different dimensions stored as pixels. A sensor per each light wavelength records the
106 reflectance of a certain object in that wavelength which are stored into numbers in a
107 certain range (e.g., digital numbers in 8 bits, ranging from 0 to 255). In general, the
108 higher the variability in the spectral space defined by the pixel reflectance values, the
109 higher the diversity of the ecosystem under study.

110 Consider a window of N pixels moving across the whole image to calculate a diversity
111 index. Let i and j be two pixels randomly chosen with repetition within the moving
112 window. Let d_{ij} be a symmetric measure of the (multi)spectral distance between i and j
113 such that $d_{ij} = d_{ji}$ and $d_{ii} = 0$. Rao's Q (Rao , 1982) is defined as:

$$Q = \sum_{i,j=1}^N p_i p_j d_{ij} = \sum_{i,j=1}^N \frac{1}{N} \times \frac{1}{N} d_{ij} \quad (3)$$

114
115 Therefore, Q measures the expected (i.e. mean) distance between two randomly
116 chosen pixels and $\frac{1}{N}$ is the probability to extract each pixel. Note that, unlike H_α or
117 K_α the calculation of Rao's quadratic entropy is not limited to single bands but can
118

1
2
3
4
5
6
7
8
9
10
11
12
13
14
15
16
17
18
19
20
21
22
23
24
25
26
27
28
29
30
31
32
33
34
35
36
37
38
39
40
41
42
43
44
45
46
47
48
49
50
51
52
53
54
55
56
57
58
59
60

118 be extended to multispectral systems of any dimension. For the connection between
119 quadratic entropy and variance, see Rocchini et al., 2019.

120 Two parametric versions of quadratic entropy have been proposed by Ricotta and
121 Szeidl (2006) and Leinster and Cobbold (2012). These parametric formulas were aimed
122 at reconciling Rao's Q with parametric entropies. However, they have only been rarely
123 used in practice.

124 A more direct approach for developing a parametric version of quadratic entropy
125 stems from the work of Guiasu and Guiasu (2011). Let $\omega_{ij} = \frac{1}{N} \times \frac{1}{N}$ be the combined
126 probability of selecting pixels i and j in this order. Guiasu and Guiasu (2011) noted that
127 Rao's Q can be expressed as a linear function of the combined probabilities of all pairs
128 of pixels:

$$Q = \sum_{i,j=1}^N \omega_{ij} d_{ij} = \sum_{i,j=1}^N \frac{1}{N} \times \frac{1}{N} d_{ij} = \sum_{i,j=1}^N \frac{1}{N^2} d_{ij} \quad (4)$$

129
130 In practice, Rao's Q is the arithmetic mean of the distances d_{ij} between all pairs of
131 pixels i and j . Hence, in order to implement a parametric version of Rao's Q , it seems
132 natural to substitute the arithmetic mean in Equation 4 with a generalized mean (Hardy
133 et al., 1952):

$$Q_\alpha = \left(\sum_{i,j=1}^N \omega_{ij} d_{ij}^\alpha \right)^{\frac{1}{\alpha}} = \left(\sum_{i,j=1}^N \frac{1}{N^2} d_{ij}^\alpha \right)^{\frac{1}{\alpha}} \quad (5)$$

134
135 This operation connects Q_α with other diversity metrics that are expressed as gener-
136 alized means, such as Hill's (Hill, 1973) or Jost's (Jost, 2006) numbers (Appendix S1)

137 equivalents (see also Leinster and Cobbold, 2012).

138 The Rao's Q , viewed as an arithmetic mean, is one of all the possible means in its
 139 generalized form Q_α :

$$Q_\alpha = \begin{cases} \alpha \rightarrow 0, Q_0 = \sqrt[N^2]{\prod_{i,j=1}^N d_{ij}} & \text{geometric} \\ \alpha = 1, Q_1 = Q = \sum_{i,j=1}^N \frac{1}{N^2} d_{ij} & \text{arithmetic} \\ \alpha = 2, Q_2 = \sqrt{\sum_{i,j=1}^N \frac{1}{N^2} d_{ij}^2} & \text{quadratic} \\ \alpha = 3, Q_3 = \sqrt[3]{\sum_{i,j=1}^N \frac{1}{N^2} d_{ij}^3} & \text{cubic} \\ \alpha \rightarrow \infty, Q_{\alpha \rightarrow \infty} = \max d_{ij} & \text{max}_d \end{cases} \quad (6)$$

140
 141 The mathematical proof that i) for $\alpha \rightarrow 0$ Q_0 corresponds to the geometric mean,
 142 and ii) for $\alpha \rightarrow \infty$ Q_∞ corresponds to the maximum distance between pixel values pairs
 143 is provided in Appendix S1.

144 Each generalized mean always lies between the smallest and largest of its values.
 145 Increasing the parameter α will increase the weight of the highest values of d_{ij} , thus
 146 providing a continuum of potential diversity indices (Figure 1).

147 3 The algorithm

Starting from a satellite image, a spatial moving window might be used to make the
 calculation on predefined extents of analysis. The grain (*sensu* Dungan et al., 2002) will
 be the resolution of the image while the extent of analysis will be the size of the moving

1
2
3 window (Figure 2). The calculation is based on a distance matrix of type:
4
5
6

$$M_d = \begin{pmatrix} d_{\lambda_1, \lambda_1} & d_{\lambda_1, \lambda_2} & d_{\lambda_1, \lambda_3} & \cdots & d_{\lambda_1, \lambda_n} \\ d_{\lambda_2, \lambda_1} & d_{\lambda_2, \lambda_2} & d_{\lambda_2, \lambda_3} & \cdots & d_{\lambda_2, \lambda_n} \\ d_{\lambda_3, \lambda_1} & d_{\lambda_3, \lambda_2} & d_{\lambda_3, \lambda_3} & \cdots & d_{\lambda_3, \lambda_n} \\ \vdots & \vdots & \vdots & \ddots & \vdots \\ d_{\lambda_n, \lambda_1} & d_{\lambda_n, \lambda_2} & d_{\lambda_n, \lambda_3} & \cdots & d_{\lambda_n, \lambda_n} \end{pmatrix} \quad (7)$$

148
149 among all the potential pairs of pixels inside the moving window. The diagonal terms
150 of the matrix (which equal zero) will have no effect for $\alpha > 0$ (Equation 6), since they
151 would enter the \sum term. On the contrary, for $\alpha \rightarrow 0$, they would enter the \prod term by
152 nullifying Q_0 .

153 We coded the proposed parameterization of Rao's quadratic entropy as an R function,
154 implementing the previously developed `rasterdiv` package (Marcantonio et al. (2020),
155 <https://CRAN.R-project.org/package=rasterdiv>). The calculation of different Q_α
156 by automatically changing the range of potential α values is done by the function `paRao`,
157 as:

```
158 > paRao(x, alpha=c(0:4, Inf), method="classic",  
159 dist_m="euclidean", window=9, na.tolerance=0.5, simplify=3,  
160 np=8, cluster.type="SOCK", diag=TRUE)
```

161 where `x` is the input dataset which can be a `RasterLayer` or a matrix class object,
162 `alpha` is the α parameter of Equation 5, which can be a single value or a vector of inte-
163 gers. In the example above, α is a vector of integers ranging from 0 to 4, plus `Inf`, which
164 in the R language is a reserved word representing positive infinity ($\alpha \rightarrow \infty$). The option

1
2
3
4 165 `method` decides if `paRao` is calculated with 1 single layer (`classic`) or with more than
5
6 166 one layer (`multidimension`). With `method="multidimension"` then `x` must be a list of
7
8 167 objects. `dist.m` is the type of distance considered in the calculation of the index, and can
9
10 168 be set to any distance class implemented in the R package `proxy`, such as `"euclidean"`,
11
12 169 `"canberra"` or `"manhattan"`. Moreover, `dist.m` can also be an user-defined matrix of
13
14
15 170 distances. However, if `method` is set to `"classic"` (unidimensional `paRao`) all distance
16
17
18 171 types reduce to the Euclidean distance. The argument `window` is the side length in cells
19
20 172 of the moving window (in this case set to 9), whereas `na.tolerance` is the proportion
21
22 173 (0-1) of NA's cell allowed in a moving window: if the proportion of NA's cells in a moving
23
24 174 window exceeds `na.tolerance` then the value of the moving window central pixel will be
25
26
27 175 NA. The option `simplify` allows to reduce the number of decimal places to ease the cal-
28
29 176 culation by reducing the number of numerical categories, i.e., if `simplify=3` only the first
30
31 177 three digits of data will be considered for the calculation of the index. `np` is the number
32
33 178 of parallel processes used in the calculation. If `np>1` then the `doParallel` package will
34
35 179 be called for parallel calculation, and `cluster.type` will indicate the type of cluster to be
36
37 180 opened (default is `"SOCK"`, `"MPI"` and `"FORK"` are the alternatives). The `diag` argument
38
39 181 refers to the diagonal term of Equation 7. It will have no effect on the function for $\alpha > 0$,
40
41
42 182 while it will nullify the value of Q_α if set to `TRUE`, as previously explained in Equation 7.
43
44
45
46
47 183
48
49
50

184 **3.1 Global test of the parametric Rao's Q variation over the** 185 **planet**

186 We applied the algorithm to a Copernicus Proba-V NDVI (Normalized Difference Vege-
187 tation Index) long term average image (June 21st 1999-2017) at 5km grain, also provided

1
2
3
4 188 in the `rasterdiv` package as a free `Rasterlayer` dataset which can be loaded by the
5
6 189 function `data()` (Figure 2). The parametric Rao algorithm can also be applied to mul-
7
8 190 tispectral data; in such a case distances are calculated in the multisystem created by
9
10 191 the values of the pixels in each axis/band. The moving window passing throughout the
11
12 192 whole image will return M_{Q_α} matrices/layers where α is the value chosen in the R function
13
14
15 193 `paRao`.

16
17
18 194 With $\alpha \rightarrow 0$ the \prod in Equation 6 leads to zeroes throughout the whole map (Figure
19
20 195 3). Increasing α will increase the weight of higher distances among different values until
21
22 196 reaching the maximum distance value for $\alpha \rightarrow \infty$. In this case the maximum turnover is
23
24 197 reached and areas with maximum β -diversity will be apparent. In this case, a multitem-
25
26 198 poral set is used (long term average NDVI from June 21st 1999-2017). Hence, areas with
27
28 199 the highest spatial and temporal turnover are enhanced, namely major mountain ridges.
29
30 200 We expect that using single frame images would lead to the enhancement of the spatial
31
32 201 component of diversity.

33
34
35
36
37 202 Since the whole process is based on distances in a spectral space between pairs of pixels
38
39 203 in terms of their “spectral characters” or in the “spectral space”, it is important to notice
40
41 204 some cornerstone aspects on the use of distances from satellite images, especially when
42
43 205 comparing different images or the same image in different times. In satellite images, the
44
45 206 measure of distances could be impacted by: ii) the use of different sensors with different
46
47 207 radiometric resolutions, as an example an 8-bit ($2^8 = 256$ values) with respect to a 16-bit
48
49 208 ($2^{16} = 65536$ values) image, or ii) the radiometric calibration which has been performed,
50
51 209 e.g. with a non-linear transform. Therefore, care should be taken when making use
52
53 210 of distances in remote sensing data, explicitly taking into account how the vector of
54
55 211 proportions between pixels belonging to some defined classes (e.g., digital numbers, DNs)
56
57
58
59
60

1
2
3
4
5
6
7
8
9
10
11
12
13
14
15
16
17
18
19
20
21
22
23
24
25
26
27
28
29
30
31
32
33
34
35
36
37
38
39
40
41
42
43
44
45
46
47
48
49
50
51
52
53
54
55
56
57
58
59
60

212 was obtained.

213 The complete code of the function can be directly seen in R by typing the `paRao`
214 function name. Moreover, a complete R coding session, to perform the above described
215 analysis is provided in Appendix S2.

216 **3.2 Local case study: the diversity of vegetation greenness and** 217 **the ecoregions of California**

218 A comparison between in-situ and remotely sensed diversity at worldwide scale might
219 be difficult due to known biases in e.g. sampling effort, taxonomies, spatial uncertainty
220 (Rocchini et al., 2017). Hence, we decided to calculate the Rao's Q index on a NDVI
221 raster layer of California (USA) to be compared with data in the field on native plant
222 species diversity provided in Thornhill et al. (2017) from Baldwin et al. (2017). We chose
223 California as a case study due to its high ecological diversity as well as to the availability
224 of plant species field-data for this region.

225 In practice, we aimed at visualizing and describing differences in both diversity and
226 structure of vegetation for the state of California, USA. First, an NDVI raster layer
227 was derived from Copernicus Sentinel-2 data (European Space Agency, reference period:
228 January 2017 to July 2018) and processed through Google Earth Engine to filter out
229 cloud cover, select the greenest pixel of the time series and resample at 100 m pixel
230 resolution. Then, the `paRao` R function was used to derive Rao's Q index, considering
231 both the original formulation of the Rao's Q ($\alpha = 1$, Equation 6) and the formulation
232 with $\alpha \rightarrow \infty$ maximizing β -diversity (Figure 3), with a moving window of 9x9 pixels.

233 A map of plant species richness was derived using the potential distribution range of
234 5,222 native California vascular plants modelled by Thornhill et al. (2017). Moreover,

1
2
3
4 235 a vector map reporting the ecoregions of California (level III) was downloaded from the
5
6 236 United States Environmental Protection Agency. In Figure 4, we showed NDVI, the Rao's
7
8 237 Q indices with $\alpha = 1$ and $\alpha \rightarrow \infty$ and plant species richness, reporting the boundaries
9
10 238 of the different ecoregions for California. This comparison revealed macro-ecological and
11
12
13 239 bio-geographical patterns which can be better interpreted considering the information
14
15 240 condensed in the Rao's Q index.

16
17
18 241 For example, the ecoregion "Coast range" (labelled with 1 in Figure 4) is composed
19
20 242 by low mountains covered by highly productive, rain-drenched evergreen forests. As a
21
22 243 result, this region showed very high NDVI values but a low Rao's Q index (low vegetation
23
24 244 structural diversity) and low to medium plant species richness. The adjacent "Klamath
25
26
27 245 Mountain" ecoregion (2) is instead characterized by highly dissected ridges, foothills,
28
29
30 246 and valleys. This region still showed high NDVI values but higher Rao's values with
31
32 247 respect to region 1, which resulted in a high plant species richness. The diverse flora of
33
34 248 this region, a mosaic of both northern Californian and Pacific Northwestern conifers and
35
36
37 249 hardwoods, is rich in endemic and relic species. A similar pattern, although caused by
38
39 250 opposite factors, was recognizable for the "Central Valley" region of California (3), which
40
41 251 is composed of flat, urbanized and intensively farmed plains. The extensive presence of
42
43
44 252 irrigated crops intersected with urbanized areas caused medium to high NDVI values and
45
46
47 253 a very high apparent structural diversity. However, the same factors caused a low native
48
49 254 species richness, especially in the drier southern portion of the valley. Finally, very dry
50
51 255 and warm broad basins and scattered mountains characterize the "Mohave and Sonora
52
53
54 256 ranges" ecoregions (4) which showed very low NDVI and Rao's Q values (with scattered
55
56 257 higher values associated with local topographical variability) and low native plant species
57
58
59 258 richness.
60

1
2
3
4 259 Passing from the pure Rao's Q index ($\alpha=1$) to its parameterization with $\alpha \rightarrow \infty$
5
6 260 helped to increase the discrimination among areas, due to the fact that when $\alpha \rightarrow \infty$
7
8 261 the Rao's Q corresponds to the maximum distance (β -diversity) among pixel values in a
9
10 262 site. Very similar gradients of the spatial heterogeneity of California (including BIOMOD
11
12 263 variables, NDVI, elevation) as well as environmental DNA (eDNA) data are found in Lin
13
14
15 264 et al. (2020).
16
17
18
19

20 265 4 Discussion

21
22
23
24 266 In this paper, we provided a straightforward solution to: i) account for distances in an
25
26 267 Information Theory based metric, and ii) provide a generalized formula in order to avoid
27
28 268 point description and account for the continuum of diversity. Diversity can be represented
29
30 269 by different dimensions (Nakamura et al., 2020). Considering one single metric to account
31
32 270 for the whole continuum of diversity metrics might be a powerful **addition** to the main
33
34 271 framework. On the contrary, fragmenting the concept of diversity when trying to capture
35
36 272 single aspects of the whole spectrum could be counterproductive.
37
38
39

40 273 The proposed unifying measure succeeded to integrate abundance- and distance-based
41
42 274 algorithms over a wide variety of diversity metrics. We demonstrated that such integra-
43
44 275 tion is not only theoretical but also applicable to real spatial data, considering several
45
46 276 dimensions of diversity at the same time. Being part of the **rasterdiv** R package, the
47
48 277 proposed method is expected to ensure high robustness and reproducibility.
49
50

51
52 278 Remote sensing is obviously not a panacea for all the organismic based diversities like
53
54 279 taxonomic-, functional-, genetic-diversity but it can represent an important exploratory
55
56 280 tool to detect diversity hotspots and their changes in space and time at the ecosystem
57
58 281 level. First of all, it measures heterogeneity of the environment with indirect links to
59
60

1
2
3 282 the biodiversity of both plant and animal taxa, but also with potential discrepancies
4
5
6 283 with species diversity, as in the presented case study of the native plant species diversity
7
8 284 of California. This said, depending on the complexity and the resolution at which the
9
10 285 proposed parameterized Rao's Q is applied, it might allow finding new insights on the
11
12 286 ecological processes acting in a certain ecosystem to shape its diversity. In this paper,
13
14
15 287 the examples provided were based on a single NDVI layer since i) it is a valuable index
16
17 288 of vegetation health and ii) it is freely available in the `rasterdiv` package to reproduce
18
19
20 289 the code proposed in this paper. We are aware that NDVI has very limited capacity
21
22 290 to track diversity in some habitats like dense forests, because it is saturated at dense
23
24
25 291 vegetation. From this point of view, imaging spectroscopy offers higher information
26
27 292 content, also enabling plant functional trait retrievals (Jetz et al., 2016; Schneider et al.,
28
29
30 293 2019) as well as structural traits by LiDAR data (Schneider et al., 2020). The application
31
32 294 of the proposed algorithm to future spaceborne imaging spectroscopy is promising. In
33
34
35 295 other words, the algorithm has been thought to be used with multiple layers, like a
36
37 296 whole multispectral image or the most meaningful Principal Components (Peres-Neto et
38
39 297 al., 2005), or land use classes probabilities derived from fuzzy set theory (Rocchini and
40
41
42 298 Ricotta, 2007; Feoli, 2018). This is even one of the major advantages of the Rao's Q
43
44 299 metric which allows considering both abundance and distance among pixel values, thus
45
46
47 300 being applicable to any continuous raster layer, or to any matrix combination, even in a
48
49 301 multiple spectral system.

50
51 302 Creating a unique "umbrella" under which all of the potential metrics of diversity can
52
53
54 303 be used is highly beneficial for e.g. monitoring the variation in time of biological systems
55
56 304 considering two major axes: i) the α parameter in Equation 5 providing information
57
58 305 about the type of diversity at time t_0 , ii) the temporal dimension from time t_0 to time t_n
59
60

1
2
3
4 306 given the same α parameter. For the future, exploring such temporal dimension would
5
6 307 allow gathering information of ecosystem changes in different diversity types at a glance.
7

8 308 Moreover, generalized entropy allows us to characterize the dimensionality of diversity
9
10 309 (*sensu* Stevens and Tello, 2014) of different habitats/ecosystems. Those areas with a
11
12 310 higher diversity dimensionality, namely a higher variability into the diversity spectrum
13
14
15 311 would need a generalized measure to be fully undertaken. On the contrary, ecosystems
16
17 312 with a lower dimensionality would have a lower difference among the different diversity
18
19 313 measures with a flat curve of the diversity spectrum (Nakamura et al., 2020).
20
21

22 314 From a functional point of view, when all indices of diversity are highly correlated to
23
24 315 each other (low dimensionality), it is expected that the ecological processes underlying
25
26 316 diversity are just a few. On the contrary, with a lower correlation among indices (higher
27
28 317 dimensionality) there might be a higher number of axes of variation coming out from
29
30 318 different processes shaping ecological heterogeneity in space (Stevens and Tello, 2014).
31
32
33

34 319 There might be the possibility that a completely random matrix produces a pattern
35
36 320 of diversity (Type I error). On the other side, a structured matrix could produce a very
37
38 321 low diversity pattern (Type II error, Gotelli (2000)). In both cases, the parametric Rao's
39
40 322 Q could allow to determine, thanks to the use of a continuum of diversities, i) why a
41
42 323 diversity pattern is still produced even in case of a random matrix, and ii) why a certain
43
44 324 landscape shows a very low diversity in a certain point of the whole diversity spectrum.
45
46
47 325 With point descriptors of diversity such inference cannot be done since the investigation
48
49 326 is limited to a small window of the entire diversity spectrum, by basically relying on a
50
51 327 single final number. In other words, the commonly asked question about what is the
52
53 328 index which best describes diversity has no certain answer (Gorelick, 2011). Hence, the
54
55 329 use of a trend of diversities will lead to the comprehension of hidden parts of the whole
56
57
58
59
60

1
2
3 330 diversity dimensionality.
4

5
6 331 Furthermore, it is expected that the ecological processes shaping diversity should act
7
8 332 at defined spatial scales (Borcard and Legendre, 2002). Hence, different diversity types of
9
10 333 the whole dimensionality spectrum are expected to show scale dependent patterns, being
11
12 334 apparent only at certain scales and not at some others. The use of a continuum allows
13
14 335 measuring the different diversity types altogether in a single step. Changing the extent
15
16 336 of analysis by different moving windows would then allow to encompass different spatial
17
18 337 structures at different scales.
19
20
21

22 338 While geographic gradients of diversity over space are [complex to catch](#) in their very
23
24 339 nature, biodiversity measurement has mainly relied in the past on few formulas which
25
26 340 represented an hegemony (Stevens et al., 2013). In this paper, we demonstrated that
27
28 341 diversity is actually multifaceted and should be necessarily approached through a gener-
29
30 342 alized approach.
31
32
33
34
35
36

37 343 **5 Conclusion**

38
39
40 344 [In order to unfold the dimensionality of diversity methods to directly account for several](#)
41
42 345 [aspects of diversity at a time are needed](#). From this point of view, generalized entropy
43
44 346 undoubtedly represents a powerful approach for mapping the diversity continuum.
45
46

47 347 Furthermore, it might be profitably used to plot multitemporal trends (see e.g. Dor-
48
49 348 nelas et al., 2014) of diversity metrics and discover previously imperceptible differences
50
51 349 when making use of single metrics (Figure 5).
52
53

54
55 350 Metrics grounded in Information Theory ensure to make use of relative abundance of
56
57 351 pixel values given the same richness in the moving window of analysis. However, distance
58
59 352 metrics allow to also account for the relative dispersion in the spectral space of the cloud
60

1
2
3 of pixels in a certain area (Laliberté et al., 2020). The proposed parameterization of the
4
5
6 Rao's Q explicitly considers the dispersion of pixel values in a spectral space (and their
7
8 relative abundance) by allowing catching the whole dimensionality of diversity.
9
10
11
12

13 6 Data availability

14
15
16 The code and the data used in this paper are based on completely Free and Open Source
17
18 Software, and they are available at the CRAN repository of the R package `rasterdiv`:
19
20 <https://CRAN.R-project.org/package=rasterdiv>.
21
22
23
24
25

26 References

- 27
28
29
30 Baldwin, B.G., Thornhill, A.H., Freyman, W.A., Ackerly, D.D., Kling, M.M., Morueta-
31
32 Holme, N., Mishler, B.D. (2017). Species richness and endemism in the native flora of
33
34 California. *American Journal of Botany*, 104: 1-15.
35
36
37
38 Borcard, D., Legendre, P. (2002). All-scale spatial analysis of ecological data by means
39
40 of principal coordinates of neighbour matrices. *Ecological Modelling*, 153: 51-68.
41
42
43
44 Dornelas, M., Gotelli, N.J., McGill, B., Shimadzu, H., Moyes, F., Sievers, C., Magurran,
45
46 A.E. (2014). Assemblage time series reveal biodiversity change but not systematic loss.
47
48 *Science*, 344: 296-299.
49
50
51
52 Evans, M.R., Grimm, V., Johst, K., Knuuttila, T., de Langhe, R., Lessells, C.M., Merz,
53
54 M., O'Malley, M.A., Orzack, S.H., Weisberg, M., Wilkinson, D.J., Wolkenhauer, O.,
55
56 Benton, T.G. (2013). Do simple models lead to generality in ecology? *Trends in Ecology*
57
58 & *Evolution*, 28: 578-583.
59
60

- 1
2
3 373 Ferrier, S., Manion, G., Elith, J., Richardson, K. (2007). Using generalized dissimilarity
4
5
6 374 modelling to analyse and predict patterns of beta diversity in regional biodiversity
7
8 375 assessment. *Diversity and Distributions*, 13: 252-264.
9
10
11 376 Dungan, J.L., Perry, J.N., Dale, M.R.T., Legendre, P., Citron-Pousty, S., Fortin, M.-J.,
12
13
14 377 Jakomulska, A., Miriti, M. and Rosenberg, M.S. (2002). A balanced view of scale in
15
16 378 spatial statistical analysis. *Ecography*, 25: 626-640.
17
18
19 379 Gillespie, T.W. (2005). Predicting woody-plant species richness in tropical dry forests: a
20
21
22 380 case study from South Florida, USA. *Ecological Applications*, 15: 27-37.
23
24
25 381 Gorelick, R. (2011). Do we have a consistent terminology for species diversity? The
26
27
28 382 fallacy of true diversity. *Oecologia*, 167: 885-888.
29
30
31 383 Null model analysis of species co-occurrence patterns. *Ecology*, 81: 2606-2621.
32
33
34 384 Goodall, D.W. (1970). Statistical ecology, p. 99-124. In Johnston, R.F., ed. Annual review
35
36 385 of ecology and systematics, Vol. 1. Annual Reviews, Palo Alto, California, USA.
37
38
39 386 Guiasu, R.C., Guiasu, S. (2011). The weighted quadratic index of biodiversity for pairs
40
41
42 387 of species: a generalization of Rao's index. *Natural Science*, 3: 795-801.
43
44
45 388 Hardy, G., Littlewood, J.E., Polya, G. (1952). *Inequalities*. Cambridge University Press,
46
47
48 389 Cambridge, UK.
49
50
51 390 Hill, M.O. (1973). Diversity and evenness: a unifying notation and its consequences.
52
53
54 391 *Ecology*, 54: 427-431.
55
56
57 392 Hobohm, C., Janisova, M., Steinbauer, M., Landi, S., Field, R., Vanderplank, S.,
58
59 393 Beierkuhnlein, C., Grytnes, J.-A., Vetaas, R.O., Fidelis, A., de Nascimento, L., Clark,
60

- 1
2
3
4 394 V.P., Fernandez-Palacios, J.M., Franklin, S., Guarino, R., Huang, J., Krestov, P., Ma,
5
6 395 K., Onipchenko, V., Palmer, M.W., Fragomeni Simon, M., Stolz, C., Chiarucci, A.
7
8 396 (2019). Global endemics-area relationships of vascular plants. *Perspectives in Ecology*
9
10 and Conservation, 17: 41-49.
11
12
13 398 Hutchinson, G. 1959. Homage to Santa Rosalia or why are there so many kinds of animals?
14
15
16 399 *American Naturalist*, 93: 145-159.
17
18
19 400 Feoli, E. (2018). Classification of plant communities and fuzzy diversity of vegetation
20
21 systems. *Community Ecology*, 19: 186-198.
22
23
24 402 Jetz, W., Cavender-Bares, J., Pavlick, R., Schimel, D., Davis, F.W., Asner, G.P., Gu-
25
26 ralnick, R., Kattge, J., Latimer, A.M., Moorcroft, P., Schaepman, M.E., Schildhauer,
27
28 403 M.P., Schneider, F.D., Schrod, F., Stahl, U., Ustin, S.L. (2016). Monitoring plant
29
30 404 functional diversity from space. *Nature Plants*, 2: 16024.
31
32
33
34 405
35 406 Johnson, P.C.D., Barry, S.J.E., Ferguson, H.M., Müller, P. (2015). Power analysis for
36
37 generalized linear mixed models in ecology and evolution. *Methods in Ecology and*
38
39 407 *Evolution*, 6: 133-142.
40
41
42
43 408
44 409 Jost, L. (2006). Entropy and diversity. *Oikos*, 113: 363-375.
45
46
47 410 Laliberté, E., Schweiger, A.K., Legendre, P: (2019). Partitioning plant spectral diversity
48
49 411 into alpha and beta components. *Ecology Letters*, 23: 370-380.
50
51
52 412 Leinster, T., Cobbold, C.A. (2012). Measuring diversity: the importance of species simi-
53
54 413 larity. *Ecology*, 93: 477-489.
55
56
57 414 Leitão, P.J., Schwieder, M., Suess, S., Catry, I., Milton, E.J., Moreira, F., Osborne, P.E.,
58
59 415 Pinto, M.J., van der Linden, S., Hostert, P. (2015), Mapping beta diversity from space:
60

1
2
3
4 416 Sparse Generalised Dissimilarity Modelling (SGDM) for analysing high-dimensional
5
6 417 data. *Methods in Ecology and Evolution*, 6: 764-771.

7
8
9 418 Lin, M., Levi Simons, A., Curd, E.E., Harrigan, R.J., Schneider, F.D., Ruiz-Ramos,
10
11 419 D.V., Gold, Z., Osborne, M.G., Shirazi, S., Schweizer, T.M., Moore, T.N., Fox, E.A.,
12
13 420 Turba, R., Garcia-Vedrenne, A.E., Helman, S.K., Rutledge, K., Palacios Mejia, M.,
14
15 421 Munguia Ramos, M.N., Wetzler, R., Pentcheff, D., McTavish, E.J., Dawson, M.N.,
16
17 422 Shapiro, B., Wayne, R.K., Meyer, R.S. (2020). A biodiversity composition map of Cali-
18
19 423 fornia derived from environmental DNA metabarcoding and Earth observation. *bioRxiv*
20
21 424 2020.06.19.160374. doi: <https://doi.org/10.1101/2020.06.19.160374>

22
23
24
25
26 425 MacArthur, R.H., Recher, H., Cody, M. (1966). On the relation between habitat selection
27
28 426 and species diversity. *American Naturalist*, 100: 319-327.

29
30
31
32 427 Marcantonio, M., Iannacito, M., Thouverai, E., Da Re, D., Tattoni, C., Bacaro, G.,
33
34 428 Vicario, S., Rocchini, D. (2020). rasterdiv: Diversity Indices for Numerical Matrices.
35
36 429 R package version 0.2-0. <https://CRAN.R-project.org/package=rasterdiv>

37
38
39
40 430 Nakamura, G., Gonçalves, L.O., Duarte, L.d.S. (2020). Revisiting the dimensionality of
41
42 431 biological diversity. *Ecography*, 43: 539-548.

43
44
45
46 432 Patil, G.P., Taillie, C. (1982). Diversity as a concept and its measurement. *Journal of the*
47
48 433 *American Statistical Association*, 77: 548-561.

49
50
51 434 Peres-Neto, P.R., Jackson, D.A., Somers, K.M. (2005). How many principal components?
52
53 435 stopping rules for determining the number of non-trivial axes revisited. *Computational*
54
55 436 *Statistics & Data Analysis*, 49: 974-997.

- 1
2
3 437 Rao, C.R. (1982). Diversity and dissimilarity coefficients: a unified approach. *Theoretical*
4
5
6 438 *Population Biology*, 21: 24-43.
7
8
9 439 Rényi, A., 1970. *Probability Theory*. North Holland Publishing Company, Amsterdam.
10
11
12 440 Ricotta, C., Szeidl, L. (2006). Towards a unifying approach to diversity measures: bridg-
13
14 441 ing the gap between the Shannon entropy and Rao's quadratic index. *Theoretical Pop-*
15
16 442 *ulation Biology*, 70: 237-243.
17
18
19
20 443 Rocchini, D., Andreini Butini, S., Chiarucci, A. (2005). Maximizing plant species inven-
21
22 444 tory efficiency by means of remotely sensed spectral distances. *Global Ecology and*
23
24 445 *Biogeography*, 14: 431-437.
25
26
27
28 446 Rocchini, D., Delucchi, L., Bacaro, G., Cavallini, P., Feilhauer, H., Foody, G.M., He,
29
30 447 K.S., Nagendra, H., Porta, C., Ricotta, C., Schmidtlein, S., Spano, L.D., Wegmann,
31
32 448 M., Neteler, M. (2013). Calculating landscape diversity with information-theory based
33
34 449 indices: A GRASS GIS solution. *Ecological Informatics*, 17: 82-93.
35
36
37
38
39 450 Rocchini, D., Garzon-Lopez, C.X., Marcantonio, M., Amici, V., Bacaro, G., Bastin, L.,
40
41 451 Brummitt, N., Chiarucci, A., Foody, G.M., Hauffe, H.C., He, K.S., Ricotta, C., Rizzoli,
42
43 452 A., Rosá, R. (2017). Anticipating species distributions: handling sampling effort bias
44
45 453 under a Bayesian framework. *Science of the Total Environment*, 584-585, 282-290.
46
47
48
49 454 Rocchini, D., Hortal, J., Lengyel, S., Lobo, J.M., Jiménez-Valverde, A., Ricotta, C.,
50
51 455 Bacaro, G., Chiarucci, A. (2011). Accounting for uncertainty when mapping species
52
53 456 distributions: The need for maps of ignorance. *Progress in Physical Geography*, 35:
54
55 457 211-226.
56
57
58
59 458 Rocchini, D., Luque, S., Pettorelli, N., Bastin, L., Doktor, D., Faedi, N., Feilhauer,

- 1
2
3
4 459 H., Féret, J.-B., Foody, G.M., Gavish, Y., Godinho, S., Kunin, W.E., Lausch, A.,
5
6 460 Leitão, P.J., Marcantonio, M., Neteler, M., Ricotta, C., Schmidtlein, S., Vihervaara,
7
8 461 P., Wegmann, M., Nagendra, H. (2018). Measuring β -diversity by remote sensing: a
9
10 462 challenge for biodiversity monitoring. *Methods in Ecology and Evolution*, 9: 1787-1798.
11
12
13
14 463 Rocchini, D., Marcantonio, M., Da Re, D., Chirici, G., Galluzzi, M., Lenoir, J., Ricotta,
15
16 464 C., Torresani, M., Ziv, G. (2019). Time-lapsing biodiversity: an open source method
17
18 465 for measuring diversity changes by remote sensing. *Remote Sensing of Environment*,
19
20
21 466 231: 111192.
22
23
24 467 Rocchini, D., Ricotta, C. (2007). Are landscapes as crisp as we may think? *Ecological*
25
26 468 *Modelling*, 204: 535-539.
27
28
29
30 469 Schimel, D., Schneider, F.D., JPL Carbon and Ecosystem Participants (2019). Flux tow-
31
32 470 ers in the sky: global ecology from space. *New Phytologist*, 224: 570-584.
33
34
35 471 Schneider, F.D., Ferraz, A., Schimel, D. (2019). Watching Earth's Interconnected Systems
36
37 472 at Work. *Eos*, 100.
38
39
40
41 473 Schneider, F.D., Ferraz, A., Hancock, S., Duncanson, L.I., Dubayah, R.O., Pavlick, R.P.,
42
43 474 Schimel, D.S. (2020). Towards mapping the diversity of canopy structure from space
44
45 475 with GEDI. *Environmental Research Letters*, 15, 115006.
46
47
48
49 476 Shannon, C.E. (1948). A mathematical theory of communication. *Bell System Technical*
50
51 477 *Journal*, 27: 379-423, 623-656.
52
53
54
55 478 Stevens, R.D., Tello, J.S. (2014). On the measurement of dimensionality of biodiversity.
56
57 479 *Global Ecology and Biogeography*, 23: 1115-1125.
58
59
60

1
2
3
4 480 Stevens, R.D., Tello, J.S., Gavilanez, M.M. (2013). Stronger tests of mechanisms under-
5
6 481 lying geographic gradients of biodiversity: insights from the dimensionality of biodi-
7
8 482 versity. PLOS ONE, 8: e56853.

9
10
11 483 [Thornhill, A.H., Baldwin, B.G., Freyman, W.A., Nosratinia, S., Kling, M.M., Morueta-
12
13 484 Holme, N., Madsen, T.P., Ackerly, D.D., Mishler, B.D. \(2017\). Spatial phylogenetics
14
15 485 of the native California flora. BMC Biology 15: 96.](#)

16
17
18
19 486 Whittaker, R.H. (1965). Dominance and diversity in land plant communities. Science,
20
21 487 147: 250-260.

22
23
24
25 488 Zellweger, F., De Frenne, P., Lenoir, J., Rocchini, D., Coomes, D. (2019). Advances in
26
27 489 microclimate ecology arising from remote sensing. Trends in Ecology & Evolution, 34:
28
29 490 327-341.

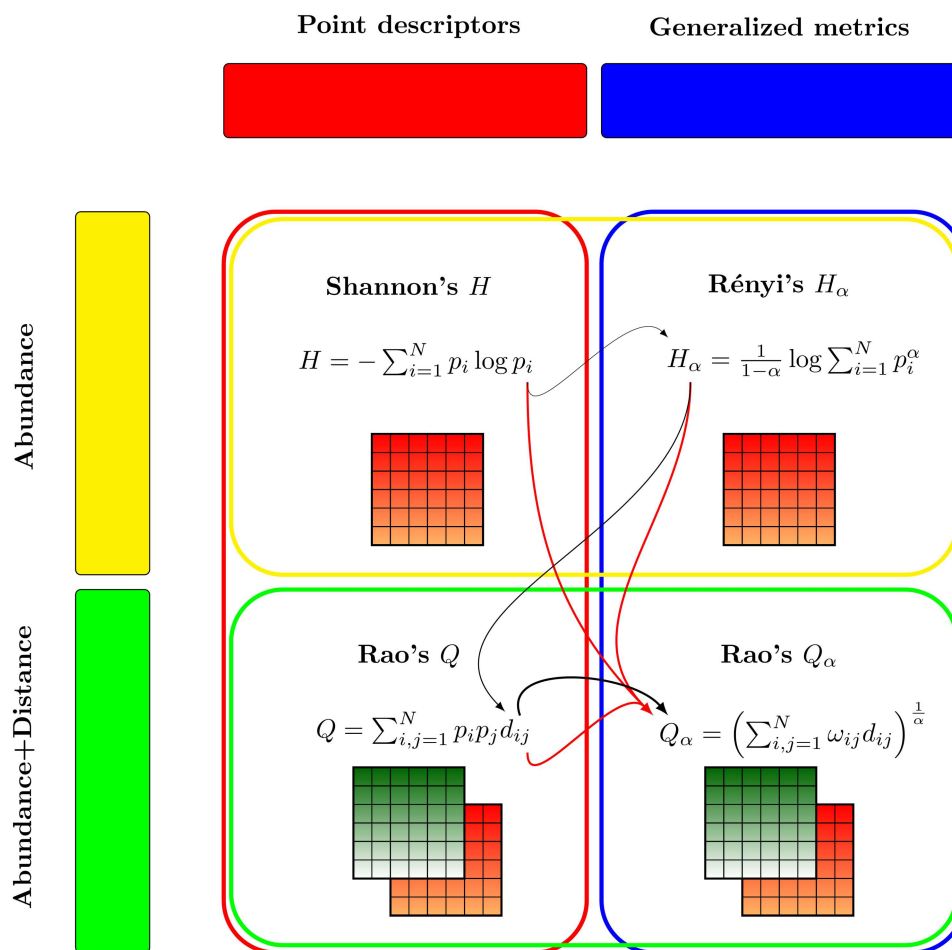
491 **Figures**

Figure 1: Grounding theory of this paper. Diversity measures can encompass abundance-based as well as abundance-distance-based metrics (yellow and green boxes, respectively). Abundance-distance-based metrics allow multiple layers to be used. The black lines represent the theoretical flow of this paper, with the thickness representing the complexity of each index, starting from Shannon's Information Theory (point descriptor) to Rényi's H_α (generalized entropy), which do not make use of distance. Distance enters the Rao's Q formula, but this is still a point descriptor of diversity. Finally, parametric Rao's Q_α comprises the use of distances and the generalized entropy concept. The red arrows represent the properties of the Rao's Q_α : i) it is grounded in Information Theory starting from Shannon's H , ii) it is a generalized entropy like the Rényi H_α , and iii) it makes use of distances like the Rao's Q .

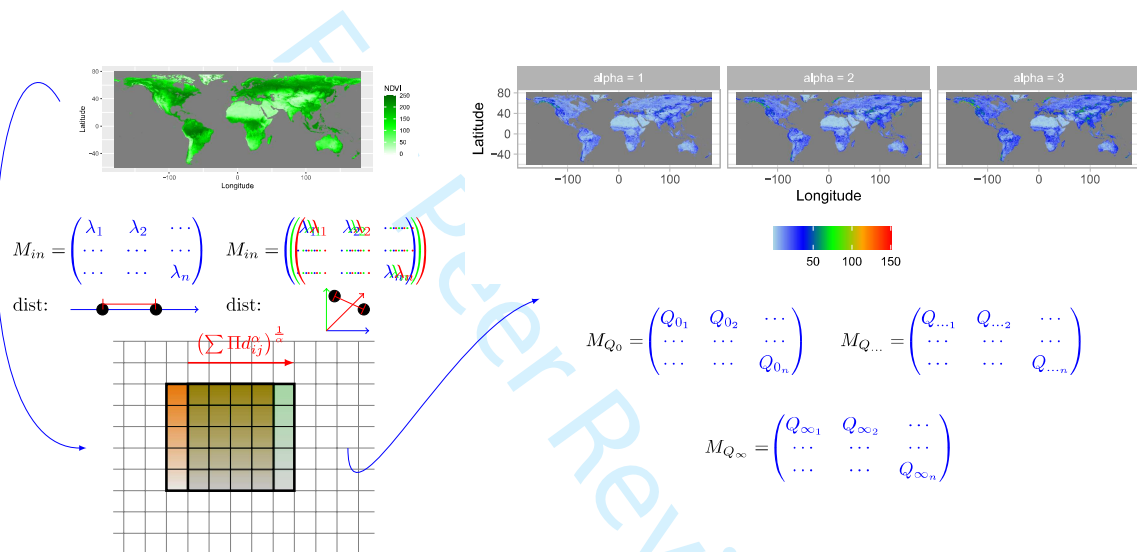


Figure 2: Starting from Copernicus Proba-V NDVI (Normalized Difference Vegetation Index) long term average image (June 21st 1999-2017) at 5km grain, parametric Rao's Q is calculated in a moving window. In this paper NDVI was used as a single layer to calculate distances on one axis, but several layers can be used as well. In this example, three layers (blue, green and red matrices) are shown to calculate distances. The algorithm is based on a moving window passing throughout the whole image, calculating the Rao's Q_{α} and saving the output in the central pixel. In this example a moving window of 5x5 pixels is passing (red arrow) from one position (orange) to the other (green). The output is a stack of layers each of which represents a different mean of the whole generalized mean spectrum of Equation 5.

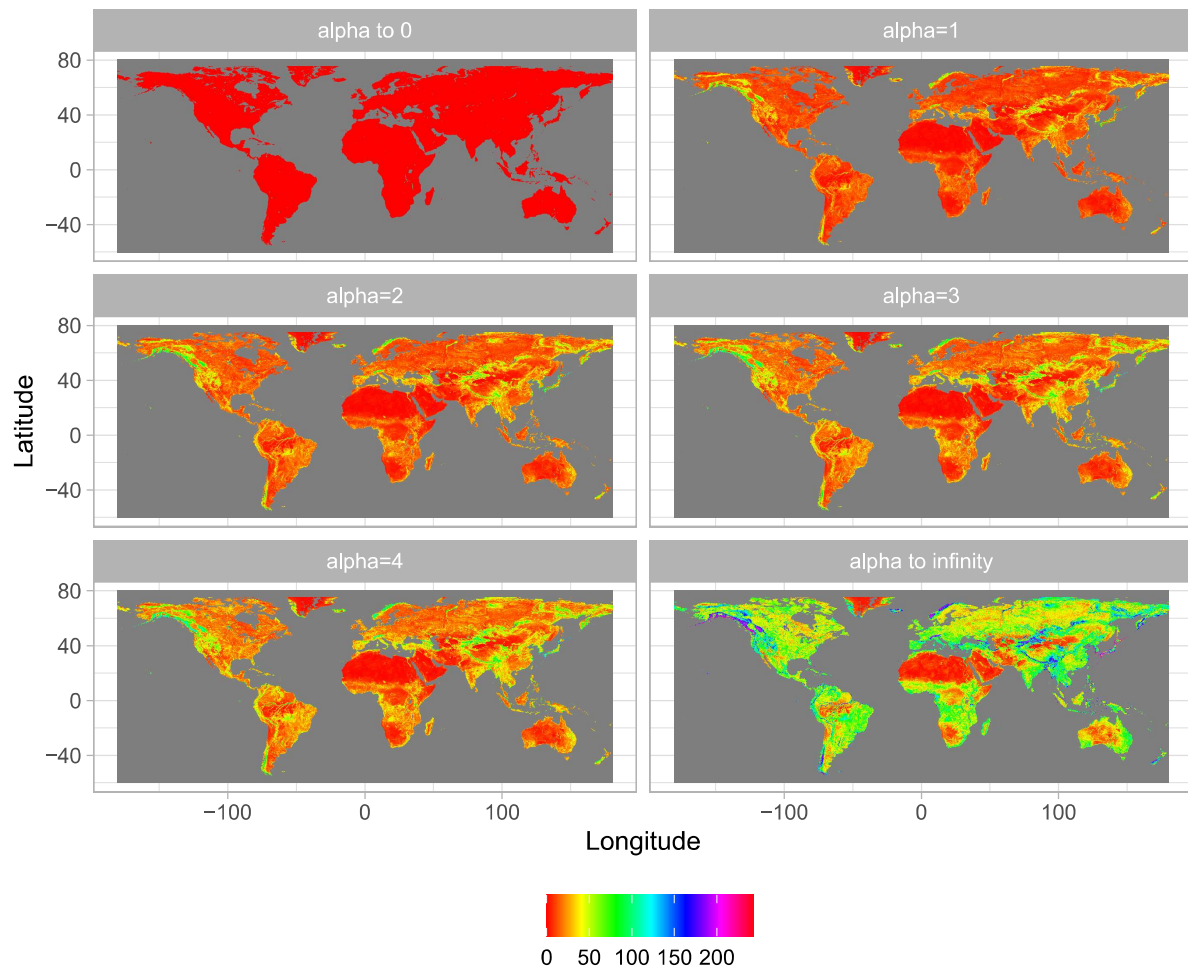


Figure 3: Output of the application of the algorithm shown in Figure 2, achieved by applying different α values: from 0 to 4 until $\alpha \rightarrow \infty$. The higher the value of the parameter α , the higher the weight of highest distances among pixel values, until reaching the maximum potential β -diversity (maximum distance) at $\alpha \rightarrow \infty$.

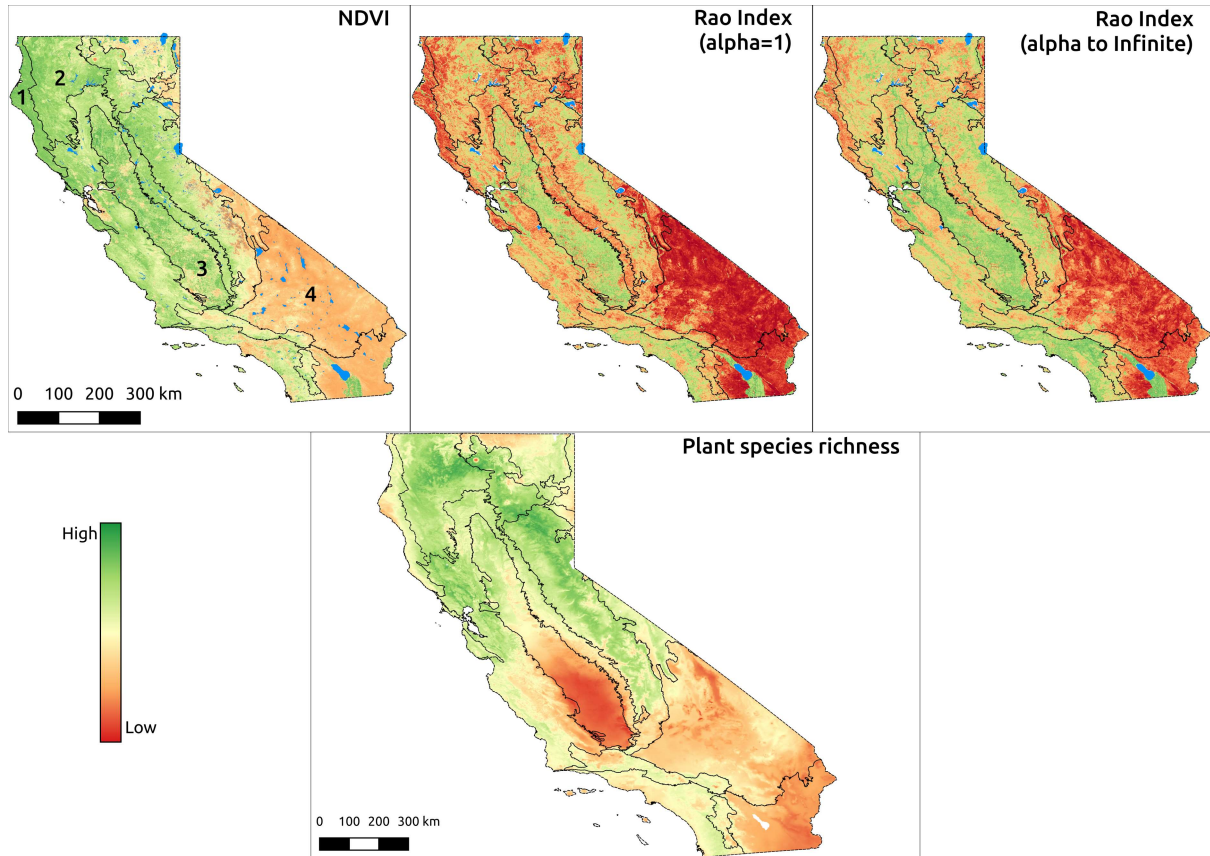
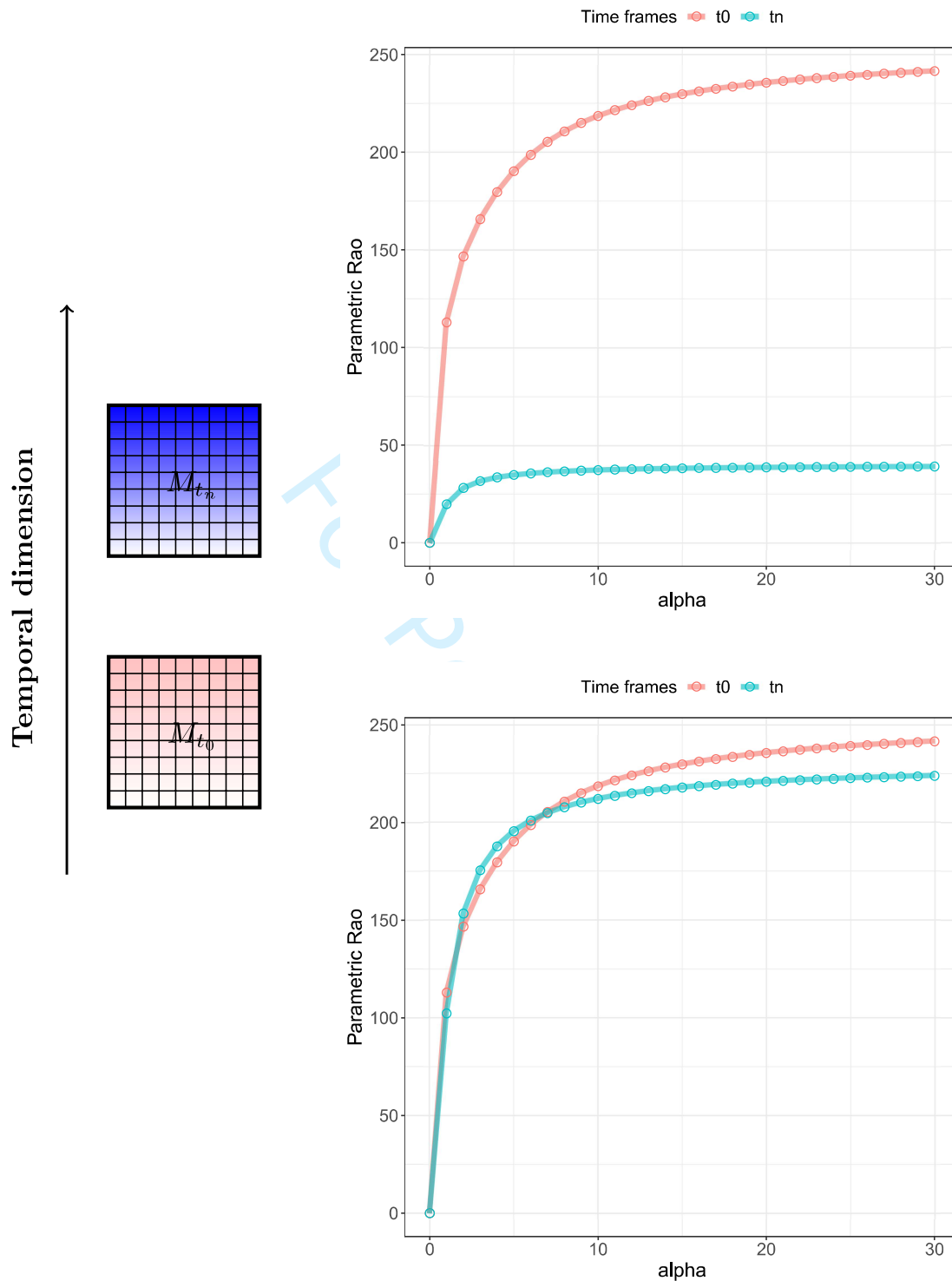


Figure 4: Comparison between NDVI, Rao's Q Index, native plant species richness for the ecoregions of California. The NDVI values shown in the top-left box (100 m resolution) were derived from the ESA Copernicus Sentinel-2 dataset then processed with Google Earth Engine and range between -0.26 (red) and 0.99 (green). The Rao's Q index shown in the top-right box was calculated from the NDVI map with $\alpha=1$ and α to infinite and a moving window of 9x9 pixels. High values are shown in dark green and represent pixel whose surrounding NDVI values are more "diverse" than pixel reported in red. The map reporting the potential native plant species richness of California (resolution: 810 m) was derived summing the binary potential distribution range of 5,222 native plant species modelled by Thornhill et al. (2017) and ranges between 134 (red) to 1029 (green) species per pixel (1 km²). The ecoregions considered in this paper are overlapped to the NDVI image: 1) Coast range (low mountains covered by highly productive, rain-drenched evergreen forests), 2) Klamath Mountain (highly dissected ridges, foothills, and valleys), 3) Central Valley (flat, urbanized and intensively farmed plains), 4) Mohave and Sonora ranges (very dry and warm broad basins).



52
53
54
55
56
57
58
59
60

Figure 5: A theoretical example of the power of using generalized entropy for monitoring purposes. Given a landscape at times t_0 (pink) and t_n (blue), calculating generalized entropy will allow the formation of a graph showing the continuum of Rao's Q values observed over a range of values for α . The same landscape in different times might show an abrupt change (e.g., a catastrophic event) with an apparent diversity decrease (top). In this case, point descriptors (e.g., single α values) of diversity may be sufficient to describe this pattern. When the change in diversity is subtle (bottom), using a point descriptor might fail to detect it but it becomes manifest in the continuum of diversities based on generalized entropy. The complete code for reproducing this theoretical example is available in Appendix S3.

1
2
3
4
5
6
7
8
9
10 1 Appendix S1 - Mathematical dissertation on the
11
12
13
14 2 proposed algorithms
15
16

17
18 3 From zero to infinity: minimum to maximum diversity
19
20
21
22 4 of the planet by spatio-parametric Rao's quadratic
23
24
25
26 5 entropy
27
28
29
30
31 6
32
33
34 7 November 7, 2020
35
36
37
38
39
40
41
42
43
44
45
46
47
48
49
50
51
52
53
54
55
56
57
58
59
60

1 Hill's numbers and generalized entropy

Hill (1973) expressed parametric diversity as the “numbers equivalent” of Rényi's generalized entropy, as:

$$K_\alpha = \frac{1}{\left(\sum_{i=1}^N p_i \times p_i^{\alpha-1}\right)^{\frac{1}{\alpha-1}}} \quad (1)$$

where the numbers equivalent K_α is the theoretical number of equally-abundant DNs (i.e. all those with $p_i = \frac{1}{K_\alpha}$) that are needed in order that its diversity be H_α (?).

Hill's K_α has the form of the reciprocal of a generalized mean of order $\alpha - 1$. Jost (2006) further showed that, like for H_α , the numbers equivalents of all parametric and non-parametric measures of diversity that can be expressed as monotonic functions of $\sum p_i^\alpha$ have the form of the reciprocal of a generalized mean of order $\alpha - 1$ (for details, Jost , 2006).

2 Mathematical proof: for $\alpha \rightarrow 0$ Q_0 is the geometric mean among the generalized means, for $\alpha \rightarrow \infty$ Q_∞ is the maximum distance between pixel values pairs

We want to compute

$$\lim_{\alpha \rightarrow 0} Q_\alpha \quad \text{where} \quad Q_\alpha = \left(\sum_{i,j=1}^N \frac{1}{N^2} d_{ij}^\alpha \right)^{\frac{1}{\alpha}} . \quad (2)$$

By $\exp(\log(x)) = x$ we can rewrite Q_α as

$$Q_\alpha = \left(\sum_{i,j=1}^N \frac{1}{N^2} d_{ij}^\alpha \right)^{\frac{1}{\alpha}} = \exp \left(\log \left(\sum_{i,j=1}^N \frac{1}{N^2} d_{ij}^\alpha \right)^{\frac{1}{\alpha}} \right) = \exp \left(\frac{1}{\alpha} \log \left(\sum_{i,j=1}^N \frac{1}{N^2} d_{ij}^\alpha \right) \right)$$

reminding that if $N > 1$, there is at least one distance $d_{ij} > 0$. We use this last expression to calculate (2). We use the following two well known results.

Theorem 1 (De l'Hôpital). *Let $f_1, g_1 : (a, b) \mapsto \mathbb{R}$ be two functions such that*

- $\lim_{x \rightarrow a} f_1(x) = \lim_{x \rightarrow a} g_1(x) = 0$
- f_1 and g_1 are differentiable in (a, b) with $g_1'(x) \neq 0$ for every $x \in (a, b)$
- the limit $\lim_{x \rightarrow a} \frac{f_1'(x)}{g_1'(x)} = L$ with $L \in \mathbb{R}$

then

$$\lim_{x \rightarrow a} \frac{f_1(x)}{g_1(x)} = L.$$

Theorem 2 (Limit composition). *Let $f_2 : (a, b) \mapsto \mathbb{R}$ and let $g_2 : (c, d) \mapsto \mathbb{R}$ be two functions such that the image set of g_2 is contained in the domain of f_2 , i.e. $\text{Img}(g_2) \subseteq (a, b)$. Let $x_0 \in (c, d)$, if it holds that*

- $\lim_{x \rightarrow x_0} g_2(x) = y_0$ with $g_2(x) \neq y_0$ definitely for $x \rightarrow x_0$
- $\lim_{y \rightarrow y_0} f_2(y) = l$

with $a, b, c, d, x_0, y_0, l \in \mathbb{R} \cup \pm\infty$ then

$$\lim_{x \rightarrow x_0} (f_2 \circ g_2)(x) = l.$$

We apply Theorem (2) to calculate the limit (2) with $f_2(x) = \exp(x)$ and

$$g_2(\alpha) = \frac{1}{\alpha} \log \left(\sum_{i,j=1}^N \frac{1}{N^2} d_{ij}^\alpha \right).$$

(all assumptions of the theorem hold). Setting $x_0 = 0$, we have to compute

$$\lim_{\alpha \rightarrow 0} g_2(\alpha). \quad (3)$$

which will be accomplished using Theorem (1) by setting $f_1 : (0, +\infty) \mapsto \mathbb{R}$

$$f_1(\alpha) = \log \left(\sum_{i,j=1}^N \frac{1}{N^2} d_{ij}^\alpha \right)$$

and $g_2 : (0, +\infty) \mapsto \mathbb{R}$, $g_2(\alpha) = \alpha$. Then we have

$$f_1(0) = \lim_{\alpha \rightarrow 0} f_1(\alpha) = \log \left(\frac{1}{N^2} \sum_{i,j=1}^N 1 \right) = \log(1) = 0$$

as the limit exists and

$$g_1(0) = \lim_{\alpha \rightarrow 0} g_1(\alpha) = 0.$$

Both functions f_1 and g_1 are differentiable. Lastly we observe that $g_1'(\alpha) \equiv 1$. Since all the assumptions of Theorem 1 hold then

$$\begin{aligned} \lim_{\alpha \rightarrow 0} \frac{f_1(\alpha)}{g_1(\alpha)} &= \lim_{\alpha \rightarrow 0} \frac{f_1'(\alpha)}{g_1'(\alpha)} = \lim_{\alpha \rightarrow 0} \frac{\left(\frac{1}{N^2} \sum_{i,j=1}^N d_{ij}^\alpha \right)^{-1} \left(\frac{1}{N^2} \sum_{i,j=1}^N d_{ij}^\alpha \log d_{ij} \right)}{1} \\ &= \frac{1}{N^2} \sum_{i,j=1}^N \log d_{ij} = \sum_{i,j=1}^N \log(d_{ij})^{\frac{1}{N^2}} = \prod_{i,j=1}^N \log(d_{ij}^{\frac{1}{N^2}}) \end{aligned} \quad (4)$$

By Equation (4) we have the expression of Equation 3. Let

$$y_0 = \prod_{i,j=1}^N \log(d_{ij}^{\frac{1}{N^2}})$$

and we conclude by observing

$$\lim_{y \rightarrow y_0} \exp(y) = \exp \left(\prod_{i,j=1}^N \log(d_{ij}^{\frac{1}{N^2}}) \right) = \prod_{i,j=1}^N \exp(\log(d_{ij}^{\frac{1}{N^2}})) = \prod_{i,j=1}^N d_{ij}^{\frac{1}{N^2}} = \sqrt[N^2]{\prod_{i,j=1}^N d_{ij}}.$$

Now we want to compute

$$\lim_{\alpha \rightarrow +\infty} Q_\alpha \quad \text{where} \quad Q_\alpha = \left(\sum_{i,j=1}^N \frac{1}{N^2} d_{ij}^\alpha \right)^{\frac{1}{\alpha}}$$

We define $d = \max\{d_{ij} | i, j \in \{1, \dots, N\}\}$ and we rewrite Q_α as

$$Q_\alpha = \left(\sum_{i,j=1}^N \frac{1}{N^2} d_{ij}^\alpha \right)^{\frac{1}{\alpha}} = \left(\sum_{i,j=1}^N \frac{1}{N^2} d^\alpha \left(\frac{d_{ij}}{d} \right)^\alpha \right)^{\frac{1}{\alpha}} = d \left(\sum_{i,j=1}^N \frac{1}{N^2} \left(\frac{d_{ij}}{d} \right)^\alpha \right)^{\frac{1}{\alpha}}$$

Next we observe that

$$\frac{d_{ij}}{d} \leq 1$$

by construction and there exist a pair (\bar{i}, \bar{j}) such that $\frac{d_{\bar{i}, \bar{j}}}{d} = 1$. Therefore it follows that

$$\sum_{i,j=1}^N \frac{1}{N^2} \left(\frac{d_{ij}}{d} \right)^\alpha = \frac{1}{N^2} \sum_{i,j=1}^N \left(\frac{d_{ij}}{d} \right)^\alpha = \frac{1}{N^2} \left(1 + \sum_{\substack{i,j=1 \\ (i,j) \neq (\bar{i}, \bar{j})}}^N \left(\frac{d_{ij}}{d} \right)^\alpha \right) \leq 1$$

for every $\alpha > 1$. And the limit in (4) is

$$\lim_{\alpha \rightarrow +\infty} d \left(\sum_{i,j=1}^N \frac{1}{N^2} \left(\frac{d_{ij}}{d} \right)^\alpha \right)^{\frac{1}{\alpha}} = d = \max_{i,j} d_{ij}.$$

1
2
3
4
5
6
7
8
9
10
11
12
13
14
15
16
17
18
19
20
21
22
23
24
25
26
27
28
29
30
31
32
33
34
35
36
37
38
39
40
41
42
43
44
45
46
47
48
49
50
51
52
53
54
55
56
57
58
59
60

34 **References**

- 35 [Hill, M.O. \(1973\). Diversity and evenness: a unifying notation and its consequences.](#)
36 [Ecology, 54: 427-431.](#)
- 37 [Jost, L. \(2006\). Entropy and diversity. Oikos, 113: 363-375.](#)

For Peer Review

1
2
3
4
5
6
7
8
9
10
11
12
13
14
15
16
17
18
19
20
21
22
23
24
25
26
27
28
29
30
31
32
33
34
35
36
37
38
39
40
41
42
43
44
45
46
47
48
49
50
51
52
53
54
55
56
57
58
59
60

1 Appendix S2 - Code

2 From zero to infinity: minimum to maximum

3 diversity of the planet by spatio-parametric

4 Rao's quadratic entropy

5
6 November 8, 2020

7 +

8 1 paRao function

```

9 function (x, dist_m = "euclidean", window = 9, alpha = 1,      1
10   method = "classic",
11   rasterOut = TRUE, lambda = 0, na.tolerance = 0, rescale =
12   FALSE,
13   diag = TRUE, simplify = 3, np = 1, cluster.type = "SOCK",  3
14   debugging = FALSE)
15 {
16   is.wholenumber <- function(x, tol = .Machine$double.eps      5
17   ^0.5) abs(x -
18     round(x)) < tol
19   if (!(is(x, "matrix") | is(x, "SpatialGridDataFrame") |
20   is(x,
21     "RasterLayer") | is(x, "list"))) {
22     stop("\nNot a valid x object.")
23   }
24   if (is(x, "SpatialGridDataFrame")) {
25     x <- raster(x)
26   }
27   else if (is(x, "matrix") | is(x, "RasterLayer")) {
28     rasterm <- x
29   }
30   else if (is(x, "list")) {
31     rasterm <- x[[1]]
32   }
33   if (na.tolerance > 1 | na.tolerance < 0) {
34     stop("na.tolerance must be in the [0-1] interval.
35   Exiting...")
36   }
37   if (any(!is.numeric(alpha))) {
38     stop("alpha must be a numeric vector. Exiting...")
39   }
40   if (any(alpha < 0)) {
41     stop("alphas must be only positive numbers. Exiting
42   ...")
43   }
44   if (method == "classic" & is(x, "RasterLayer")) {
45     isfloat <- FALSE
46     if (!is.wholenumber(rasterm@data@min) | !is.
47     wholenumber(rasterm@data@max) |
48     is.infinite(rasterm@data@min) | !is.wholenumber(
49     median(getValues(rasterm)),

```


1
2
3
4
5
6
7
8
9
10
11
12
13
14
15
16
17
18
19
20
21
22
23
24
25
26
27
28
29
30
31
32
33
34
35
36
37
38
39
40
41
42
43
44
45
46
47
48
49
50
51
52
53
54
55
56
57
58
59
60

```

50         na.rm = T))) {
51         message("Input data are float numbers. Converting
52 x data in an integer matrix...")
53         isfloat <- TRUE
54         mfactor <- 100^simplify
55         rasterm <- getValues(rasterm) * mfactor
56         rasterm <- as.integer(rasterm)
57         rasterm <- matrix(rasterm, nrow(x), ncol(x),
58 byrow = TRUE)
59         gc()
60     }
61     else {
62         rasterm <- matrix(getValues(rasterm), ncol = ncol
63 (x),
64         nrow = nrow(x), byrow = TRUE)
65     }
66     message("Matrix check OK: \nParametric Rao output
67 matrix will be returned")
68 }
69 else if (method == "classic" & (is(x, "matrix") | is(x, "
70 list")))) {
71     isfloat <- FALSE
72     if (!is.integer(rasterm)) {
73         message("Input data are float numbers. Converting
74 x in an integer matrix...")
75         isfloat <- TRUE
76         mfactor <- 100^simplify
77         rasterm <- as.integer(rasterm * mfactor)
78         rasterm <- matrix(rasterm, nrow(x), ncol(x),
79 byrow = TRUE)
80         gc()
81     }
82     else {
83         rasterm <- as.matrix(rasterm)
84     }
85     message("Matrix check OK: \nParametric Rao output
86 matrix will be returned")
87 }
88 else ("The class of x is not recognized. Exiting...")
89 if (window%%2 == 1) {
90     w <- (window - 1)/2
91 }
92 else {
93     stop("The size of the moving window must be an odd
94 number. Exiting...")
95 }
96 if (np == 1) {
97     if (method == "classic") {

```

1
2
3
4
5
6
7
8
9
10
11
12
13
14
15
16
17
18
19
20
21
22
23
24
25
26
27
28
29
30
31
32
33
34
35
36
37
38
39
40
41
42
43
44
45
46
47
48
49
50
51
52
53
54
55
56
57
58
59
60

```

98         out <- lapply(alpha, paRaoS, rasterm = rasterm, w 73
99         = w,
100             dist_m = dist_m, na.tolerance = na.tolerance,
101             diag = diag, debugging = debugging, isfloat = 75
102             isfloat,
103             mfactor = mfactor)
104     } 77
105     else if (method == "multidimension") {
106         out <- lapply(alpha, mpaRaoS, x = x, rasterm = 79
107         rasterm,
108         w = w, dist_m = dist_m, na.tolerance = na.
109         tolerance,
110         rescale = rescale, lambda = lambda, diag = 81
111         diag,
112         debugging = debugging)
113     } 83
114     if (rasterOut == T & class(x) == "RasterLayer") {
115         outR <- lapply(out, raster, template = x) 85
116         return(outR)
117     } 87
118     else {
119         return(out) 89
120     }
121 } 91
122 else if (np > 1) {
123     if (method == "multidimension") { 93
124         stop("Multidimensional paRao not yet implemented,
125         set 'np=1'. Exiting...")
126     } 95
127     else {
128         message("\n##### Starting 97
129         parallel calculation #####")
130         if (debugging) {
131             cat("#check: Before parallel function.") 99
132         }
133         if (cluster.type == "SOCK" || cluster.type == " 101
134         FORK") {
135             cls <- makeCluster(np, type = cluster.type,
136             outfile = "",
137             useXDR = FALSE, methods = FALSE, output = " 103
138             ")
139         }
140         else if (cluster.type == "MPI") { 105
141             cls <- makeCluster(np, outfile = "", useXDR =
142             FALSE,
143             methods = FALSE, output = "") 107
144         }
145         else { 109

```

```

146         message("Wrong definition for 'cluster.type'.
147 Exiting...")
148     }
149     doParallel::registerDoParallel(cls)
150     on.exit(stopCluster(cls))
151     gc()
152     out <- lapply(alpha, paRaoP, rasterm = rasterm, w
153 = w,
154         dist_m = dist_m, na.tolerance = na.tolerance,
155         diag = diag, debugging = debugging, isfloat =
156 isfloat,
157         mfactor = mfactor)
158     if (rasterOut == T & class(x) == "RasterLayer") {
159         outR <- lapply(out, raster, template = x)
160         return(outR)
161     }
162     else {
163         return(out)
164     }
165 }
166 }
167 }

```

2 Application of the paRao function to a synthetic set

```

170 # install standalone rasterdiv
171 install.packages('rasterdiv_0.2-0.tar.gz', repos = NULL, type
172 = "source")
173
174 library(raster)
175 library(rasterdiv)
176
177 # generate matrix
178 synth <- raster(ncol = 8, nrow = 8, xmn = 1, xmx = 6, ymn =
179 1, ymx = 6)
180 values(synth) <- rpois(ncell(synth), lambda=3)
181
182 # paRao function, using the code in the manuscript
183 synth.parao <- paRao(synth, alpha = c(0:4,30^9), dist_m = "
184 euclidean", window = 9, na.tolerance = 0.5, simplify = 3,
185 diag = T, rasterOut = T)

```

3 Application of the paRao function to the 8bit copNDVI dataset

```

188 library(rasterdiv)
189
190 st <- paRao(copNDVI, alpha = c(0:4,Inf),
191   dist_m = "euclidean", window = 9, na.tolerance = 0.5,
192   simplify = 3, diag = TRUE, rasterOut = TRUE)

```

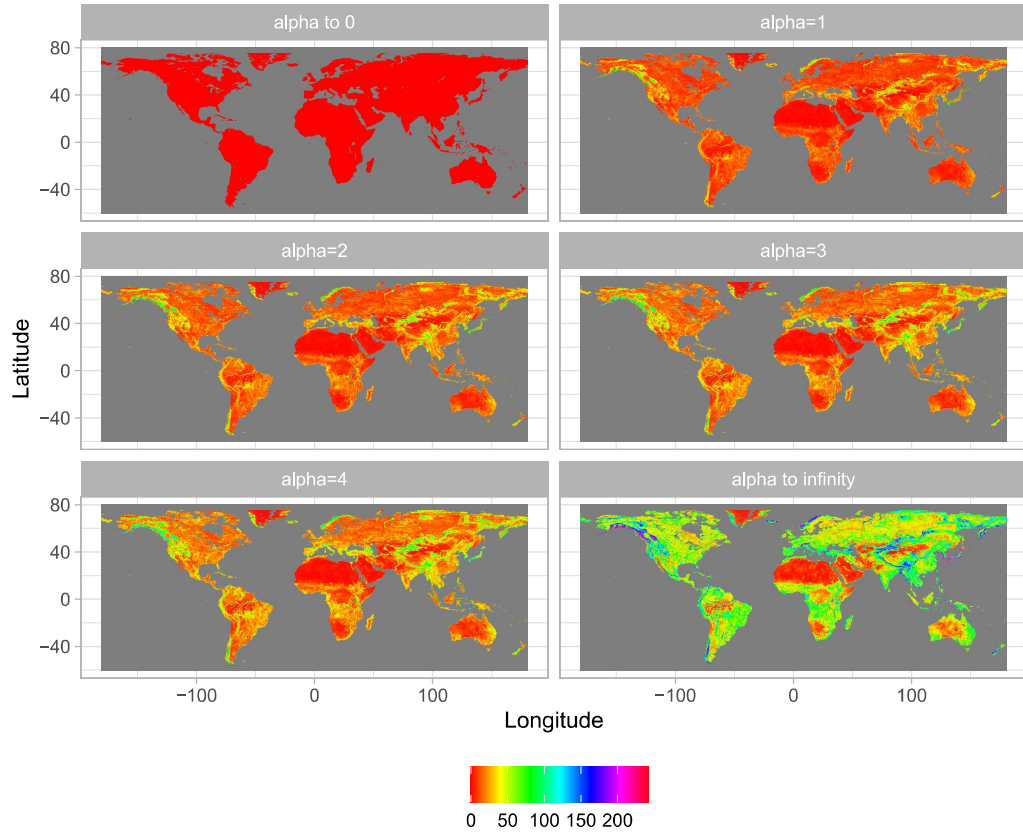
4 Output plot

```

194 library(raster)
195 library(ggplot2)
196 library(rasterVis)
197 library(RColorBrewer)
198
199 var.labs=c("layer.1" = "alpha to 0", "layer.2" = "alpha=1", "
200   layer.3" = "alpha=2", "layer.4" = "alpha=3", "layer.5" = "
201   alpha=4", "layer.6" = "alpha to infinity")
202
203 gplot(st, maxpixels=500000) +
204   geom_raster(aes(fill = value), color = "black") +
205   labs(x="Longitude",y="Latitude", fill="")+
206   scale_fill_gradientn(colors=rainbow(100)) +
207   coord_equal()+
208   theme_light()+
209   facet_wrap(~ variable, ncol = 2, labeller = labeller(
210     variable = var.labs))+
211   theme(legend.position = "bottom") +
212   NULL

```

1
2
3
4
5
6
7
8
9
10
11
12
13
14
15
16
17
18
19
20
21
22
23
24
25
26
27
28
29
30
31
32
33
34
35
36
37
38
39
40
41
42
43
44
45
46
47
48
49
50
51
52
53
54
55
56
57
58
59
60



213

iew

1
2
3
4
5
6
7
8
9
10
11
12
13
14 1 Appendix S3 - Code for Figure 4
15
16
17
18 2 From zero to infinity: minimum to maximum
19
20
21
22 3 diversity of the planet by spatio-parametric
23
24
25
26 4 Rao's quadratic entropy
27
28
29
30
31 5
32
33
34 6 June 8, 2020
35
36
37
38
39
40
41
42
43
44
45
46
47
48
49
50
51
52
53
54
55
56
57
58
59
60

```

7
8
9
10 library(ggplot2)
11 library(rasterdiv)
12 x1 <- matrix(c(255, 128, 1, 255, 128, 1, 255, 128, 1),ncol=3)
13 x2 <- matrix(c(10, 10, 10, 10, 50, 50, 50, 50, 50),ncol=3)
14 p1 <- paRao(x1,window=3,np=1,na.tolerance=0.1,dist_m="
15 euclidean",alpha=2)
16 p2 <- paRao(x2,window=3,np=1,na.tolerance=0.1,dist_m="
17 euclidean",alpha=2)
18 alphas <- seq(0,30,1)
19 out1 <- paRao(x1,window=3,np=1,na.tolerance=0.1,dist_m="
20 euclidean",alpha=alphas)
21 out2 <- paRao(x2,window=3,np=1,na.tolerance=0.1,dist_m="
22 euclidean",alpha=alphas)
23 r1 <- sapply(out1, function(y) {y[2,2]})
24 r2 <- sapply(out2, function(y) {y[2,2]})
25 ggp <- rbind.data.frame(
26   cbind.data.frame(raop=r1,alphas,"Time frames"=rep("t0",length
27     (alphas))),
28   cbind.data.frame(raop=r2,alphas,"Time frames"=rep("tn",length
29     (alphas))))
30 pdf("landscapes.pdf")
31 ggplot(ggp, aes(x=alphas, y=raop,col='Time frames')) +
32   geom_line(size=2,alpha=0.6) +
33   geom_point(cex=3,pch=21) +
34   theme_bw() +
35   xlab("alpha") +
36   ylab("Parametric Rao") +
37   theme(axis.text.x = element_text(size=14), axis.text.y =
38     element_text(size=14)) +
39   theme(axis.title.x = element_text(size=16), axis.title.y
40     = element_text(size=16))+
41   theme(legend.position="top",legend.title=element_text(
42     size=14),legend.text=element_text(size=14))
43 dev.off()
44
45
46 #####
47
48 #### Second graph
49
50 library(raster)
51 library(rasterdiv)
52 library(ggplot2)
53
54 x1 <- matrix(c(255, 128, 1, 255, 128, 1, 255, 128, 1),ncol=3)
55 x2 <- matrix(c(10, 10, 10, 10, 50, 50, 50, 50, 50),ncol=3)

```

1
2
3
4
5
6
7
8
9
10
11
12
13
14
15
16
17
18
19
20
21
22
23
24
25
26
27
28
29
30
31
32
33
34
35
36
37
38
39
40
41
42
43
44
45
46
47
48
49
50
51
52
53
54
55
56
57
58
59
60

```

56 x3 <- matrix(c(rep(20,3),rep(250,6)),ncol=3)
57 alphas <- seq(0,30,1)
58 out1 <- paRao(x1,window=3,np=1,na.tolerance=0.1,dist_m="
59   euclidean",alpha=alphas)
60 out2 <- paRao(x2,window=3,np=1,na.tolerance=0.1,dist_m="
61   euclidean",alpha=alphas)
62 out3 <- paRao(x3,window=3,np=1,na.tolerance=0.1,dist_m="
63   euclidean",alpha=alphas)
64 r1 <- sapply(out1, function(y) {y[2,2]})
65 r2 <- sapply(out2, function(y) {y[2,2]})
66 r3 <- sapply(out3, function(y) {y[2,2]})
67 ggp <- rbind.data.frame(
68   cbind.data.frame(raop=r1,alphas,"Time frames"=rep("t0",length
69     (alphas))),
70   cbind.data.frame(raop=r3,alphas,"Time frames"=rep("tn",length
71     (alphas))))
72
73 pdf("landscapes2.pdf")
74 ggplot(ggp, aes(x=alphas, y=raop,col='Time frames')) +
75   geom_line(size=2,alpha=0.6) +
76   geom_point(cex=3,pch=21) +
77   theme_bw() +
78   xlab("alpha") +
79   ylab("Parametric Rao") +
80   theme(axis.text.x = element_text(size=14), axis.text.y =
81     element_text(size=14)) +
82   theme(axis.title.x = element_text(size=16), axis.title.y
83     = element_text(size=16))+
84   theme(legend.position="top",legend.title=element_text(
85     size=14),legend.text=element_text(size=14))
86   ggsave("~/paRao_comparison1.png",dpi=600,scale=0.5,width
87     =10,height=10)
88 dev.off()

```


1
2
3
4
5
6
7
8
9
10
11
12
13
14
15
16
17
18
19
20
21
22
23
24
25
26
27
28
29
30
31
32
33
34
35
36
37
38
39
40
41
42
43
44
45
46
47
48
49
50
51
52
53
54
55
56
57
58
59
60

Temporal dimension

